





Polarized ZZ pairs in gluon fusion and vector boson fusion at the LHC

Martina Javurkova ^{a,b}, Richard Ruiz ^c, Rafael Coelho Lopes de Sá ^a, Jay Sandesara ^a

^aPhysics Department – University of Massachusetts Amherst, Amherst, Massachusetts, USA

^bPhysics Department – Matej Bel University, Tajovského 40, Banská Bystrica, 97401, Slovakia

^cInstitute of Nuclear Physics – Polish Academy of Sciences (IFJ PAN), ul. Radzikowskiego, Kraków, 31-342, Poland

Abstract

Pair production of helicity-polarized weak bosons ($V_\lambda = W_\lambda^\pm, Z_\lambda$) from gluon fusion ($gg \rightarrow V_\lambda V_{\lambda'}$) and weak boson fusion ($V_1 V_2 \rightarrow V_\lambda V_{\lambda'}$) are powerful probes of the Standard Model, new physics, and properties of quantum systems. Measuring cross sections of polarized processes is a chief objective of the Large Hadron Collider’s (LHC) Run 3 and high luminosity programs, but progress is limited by the simulation tools that are presently available. We propose a method for computing polarized cross sections that works by directly modifying Feynman rules instead of (squared) amplitudes. The method is applicable to loop-induced processes, and can capture the interference between arbitrary polarization configurations, interference with non-resonant diagrams, as well as off-shell/finite-width effects. By construction, previous results that work at the (squared) amplitude level are recoverable. As a demonstration, we report the prospect of observing and studying polarized $Z_\lambda Z_{\lambda'}$ pairs when produced via gluon fusion and electroweak processes in final-states with four charged leptons at the LHC, using the new method to simulate the gluon fusion process. Our Feynman rules are publicly available as a set of *Universal FeynRules Object* libraries called `SM_Loop_VPolar`.

Keywords: Large Hadron Collider, Helicity Polarization, Monte Carlo Tools, Multiboson Systems

1. Introduction

Helicity-polarized vector bosons in the Standard Model (SM) carry information about the mechanism of electroweak (EW) symmetry breaking (EWSB) and its role in ensuring unitarity in the model. Measurements of polarized vector states subsequently provide experimental tests of fine, structural cancellations in the SM. They can also be used to probe extensions of the SM, such as extended gauge theories [1–5], composite Higgs models [6–15], generic anomalous couplings [16, 17], as well as quantum properties of multiboson systems [18–22]. Such sensitivity holds even in the decoupling limits [23], where it is challenging for direct searches. Consequently, any program aiming to explore EWSB and new physics in the Higgs sector at the Large Hadron Collider (LHC) and future collider experiments will involve measuring polarized vector bosons [24–29].

Despite the physics needs and motivations, there is a limited supply of predictions for integrated (σ) and differential ($d\sigma$) cross sections for

TeV-scale proton (p) collisions with intermediate or final-state helicity-polarized particles, e.g.,

$$pp \rightarrow V_\lambda V_{\lambda'} (V_{\lambda''}) \quad \text{for } V \in \{W^\pm, Z, \gamma\}. \quad (1)$$

Here and throughout, λ denotes the helicity of V and q is its momentum. Predictions are notably scarce beyond tree level in perturbation theory.

Typically, helicity-polarized cross sections are obtained by first constructing the matrix elements (or their square) for an unpolarized process, and then decomposing the numerator of an intermediate, resonant propagator V into the outer product of one or more pairs of polarization vectors (or spinors for fermions). This is known generically as the “truncated-propagator” method.

With the so-called double-pole approximation (DPA) [30–33], also known as the on-shell projection (OSP) technique, non-resonant diagrams are neglected and momenta q in the numerators of propagators are “projected” to be on mass shell. (q^2 factors in the denominators are unmodified.) Dedicated predictions up to next-to-leading order (NLO) in both EW and quantum chromodynamics (QCD) are available [34–38] as are predictions up to next-to-next-to-leading order (NNLO) in QCD [39, 40]. However, these state-of-the-art predictions are limited to at most two intermedi-

martina.javurkova@cern.ch (contact author),
 rruiz@ifj.edu.pl, rclsa@umass.edu,
 jsandesara@umass.edu

ate, helicity-polarized weak bosons. Leading order (LO) event generators employing DPA/OSP are available, but again are mostly restricted to select processes [41–45].

By combining discrete Monte Carlo sampling over helicities with the spin-correlated narrow width approximation (NWA), a generalization of the truncated-propagator method was developed [46] that did not require modifying intermediate momenta. This led to the automation of helicity-polarized cross sections at LO for arbitrary tree-level processes [46]. More recently, the computation of polarized cross sections with the NWA was automated at (approximately) NLO in QCD for arbitrary processes by projecting unpolarized cross section onto a basis of polarizations, and hence providing polarized cross sections [45].

We attempt to advance this program by proposing another method for computing polarized cross sections that extends the truncated-propagator method to individual Feynman rules. The broad idea is that the (coherent/interfering) sum of polarizations of a *single, unpolarized* intermediate vector boson can be realized as the (coherent/interfering) sum of *several, polarized* states. In other words, the graph of a vector boson (or fermion) can be split into the sum of several propagating states. Polarized cross sections that include full off-shell effects, interference with non-resonant contributions, polarized t -channel contributions, and loop-induced contributions can then be obtained via diagram selection, which is a common technique in realistic simulations for the LHC.

As a demonstration and using publicly available Monte Carlo (MC) simulation tools, we use the new method to estimate the sensitivity of the LHC experiments to helicity-polarized ZZ pairs produced via gluon fusion (ggF). We also estimate the sensitivity to EW processes, including weak boson fusion (VBF) and annihilation channels. We focus on the data set sizes expected by the end of the LHC’s Run 3 era of operations and with the full dataset of the high-luminosity (HL) LHC.

This work continues as follows: In Sec. 2 we describe our proposed method for computing polarized cross sections and its practical implementation. In Sec. 3 we present LHC predictions for the production of $Z_\lambda Z_{\lambda'}$ pairs from gluon fusion. In Sec. 4 we present our projections for measuring polarized ZZ cross sections. Further applications are discussed in Sec. 5, and we conclude in Sec. 6. [Appendix A–Appendix C](#) contain additional technical details to reproduce our work.

2. Helicity polarization as a Feynman rule

After EWSB, the propagator of a massive, on-shell gauge boson V with momentum q and mass M_V is related to its polarization vectors (ε) in the Unitary gauge by the completeness relationship

$$g_{\mu\nu} - q_\mu q_\nu / M_V^2 = \sum_{\lambda \in \{0, \pm 1\}} \varepsilon_\mu(q, \lambda) \varepsilon_\nu^*(q, \lambda). \quad (2)$$

The sum runs over the longitudinal ($\lambda = 0$) and transverse ($\lambda = \pm$) states of V . Eq. (2) can be extended to off-shell V by extending the sum to the so-called “auxiliary/scalar” polarization ($\lambda = A$), and to the t -channel production by including $\lambda = A$ and summing over $(-1) \times \varepsilon_\mu(\lambda = 0) \varepsilon_\nu^*(\lambda = 0)$ instead of $(+1) \times \varepsilon_\mu(\lambda = 0) \varepsilon_\nu^*(\lambda = 0)$ [47, 48]. Strictly speaking, the helicity of V in a particular frame is only well-defined, and hence experimentally accessible, when V is on shell. This is because helicity labels an eigenstate in the mass basis and off-shell states are not eigenstates of this basis. However, in particular circumstances [49], Eq. (2) is also meaningful for t -channel exchanges [50–52].

The decoherence of a heavy object’s helicity when off-shell is evident in its propagator, which can be identified as a *coherent* sum of external polarization vectors (or spinors for fermions). That is to say, using Eq. (2) one can express the propagator of V (with mass and width M_V, Γ_V) as

$$\Pi_{\mu\nu}^V(q) = \frac{-i(g_{\mu\nu} - q_\mu q_\nu / M_V^2)}{q^2 - M_V^2 + iM_V \Gamma_V} \quad (3)$$

$$= \sum_{\lambda \in \{0, \pm 1, A\}} \eta_\lambda \left(\frac{-i\varepsilon_\mu(q, \lambda) \varepsilon_\nu^*(q, \lambda)}{q^2 - M_V^2 + iM_V \Gamma_V} \right). \quad (4)$$

Here, $\eta_\lambda = +1$, unless $\lambda = 0$ and V_λ is in the t -channel; in that case $\eta_\lambda = -1$. In Ref. [46], the quantity in the summation of Eq. (4) is labeled the “helicity-truncated” propagator $\Pi_{\mu\nu}^{V\lambda}$,

$$\Pi_{\mu\nu}^{V\lambda}(q) = \frac{-i\varepsilon_\mu(q, \lambda) \varepsilon_\nu^*(q, \lambda)}{q^2 - M_V^2 + iM_V \Gamma_V}. \quad (5)$$

Helicity-polarized matrix elements, and hence helicity-polarized cross sections ($d\sigma_\lambda$), can then be defined by using the truncated propagator of Eq. (5). The unpolarized (\mathcal{M}) and polarized (\mathcal{M}_λ) matrix elements are related by summing over λ :

$$\mathcal{M} = \mathcal{M}_f^\mu \left(\sum_{\lambda \in \{\pm 1, 0, A\}} \eta_\lambda \times \Pi_{\mu\nu}^{V\lambda} \right) \mathcal{M}_i^\nu \quad (6)$$

$$= \sum_{\lambda \in \{\pm 1, 0, A\}} \eta_\lambda \times \underbrace{\mathcal{M}_f^\mu \cdot \Pi_{\mu\nu}^{V\lambda} \cdot \mathcal{M}_i^\nu}_{=\mathcal{M}_\lambda}. \quad (7)$$

Here, \mathcal{M}_i^μ and \mathcal{M}_f^ν are the Green’s functions (diagram fragments) that sandwich the full propagator V , i.e., Eq. (3), in the unpolarized matrix element.

After squaring the polarized matrix element and integrating over phase space one obtains $d\sigma_\lambda$. The difference between the unpolarized cross section ($d\sigma_{\text{unpol.}}$) and summing over all polarized cross sections is the interference between helicity states,

$$d\sigma_{\text{unpol.}} = \sum_{\lambda \in \{\pm 1, 0, A\}} d\sigma_\lambda + \sum_{\lambda, \lambda'} \underbrace{\text{interference}}_{\mathcal{O}(\Re[\mathcal{M}_i^* \mathcal{M}_{i'}])}. \quad (8)$$

The “interference” term here also includes the contribution from non-resonant diagrams.

The magnitude of the interference is process dependent but can be incorporated by adjusting the definition of $\Pi_{\mu\nu}^{V\lambda}$ in Eq. (5) to include multiple polarizations [46]. For example: one can define the “transverse” propagator $\Pi_{\mu\nu}^{VT}$ as the sum over the $\lambda = \pm 1$ states. The interference is also phase-space dependent, the impact of which can be adjusted by restrictions on external and intermediate momenta. Finally, the accuracy of $d\sigma_\lambda$ depends on how many intermediate states are polarized.

The traditional truncated-propagator method has several advantages: (i) off-shell effects are included, (ii) it is generalizable to fermions and high-spin states, (iii) interference between polarizations can be included, and (iv) it is applicable to tree- and loop-level processes. A significant disadvantage, however, is the need to modify the propagator routines (software libraries) in existing event generators. Such work is technically challenging to implement into event generators capable of simulating arbitrary processes because the mappings between particles, their Feynman graphs, and their propagators are typically hard coded. Alterations can lead to undesired consequences for unpolarized subgraphs [45, 46].

To ameliorate this difficulty, we propose treating the truncated propagator in Eq. (5) as a Feynman rule itself. If one considers the decomposition of a state V as a combination of polarized states V_λ ,

$$|V(q, M_V)\rangle = \sum_{\lambda \in \{\pm 1, 0, A\}} |V_\lambda(q, M_V, \lambda)\rangle, \quad (9)$$

and propagates this throughout a Lagrangian, then graphically one can make the identification:

$$\frac{-i \varepsilon_\mu(q, \lambda) \varepsilon_\nu^*(q, \lambda)}{q^2 - M_V^2} = \text{wavy line} \quad V_\lambda(q). \quad (10)$$

That is, the truncated propagator $\Pi_{\mu\nu}^{V\lambda}$ in Eq. (5) is the propagator of a vector that has a fixed polar-

ization. One can then interpret Eq. (6) as the amplitude for a process that is mediated by a single particle V with interfering polarizations λ and interpret Eq. (7) as the sum of interfering diagrams for a process mediated by a *collection of particles* V_λ , where each V_λ has its own propagator. This identification is one chief result of our work.

The key to realizing this approach in realistic simulations is the fact that modern, multi-purpose event generators are sufficiently flexible to handle new Feynman rules¹, including alternative propagators, as *input* libraries. Passing Eq. (10) or Eq. (5) to event generators as an input library is an efficient alternative to modifying the built-in propagators for SM particles, which are typically hard-coded. Moreover, this method is compatible with the automated computation of so-called R_2 and ultraviolet counter-terms at NLO in QCD [57]. Therefore, “polarization as a Feynman rule” is also applicable to automated loop-induced processes.

As a brief comment, treating polarization as a Feynman rule raises the prospect that new rules are not individually Lorentz invariant, and that all external-particle momenta must be written in the same frame through the whole flow of a numerical calculation. In general, individual Feynman rules are inherently not Lorentz invariant: many rules in the SM carry spinor or vector indices. As a consequence, numerical implementations of the helicity amplitude method for computing matrix elements (for example: HELAS [58] as implemented in MadGraph [59]) already require a reference frame to be chosen before phase space integration. For LO predictions in mg5amc, including those that are loop-induced, helicity amplitudes are evaluated by default in the partonic frame, though other choices of frame are possible [46]. Our method does not change this operation; rather, the method relies and exploits these generator-dependent capabilities (and their numerical efficiencies).

2.1. Practical Implementation

To implement our proposal, we start from the default implementation of the full SM Lagrangian into FeynRules [53–56]. We add four new “particles” to the model: V_T , V_0 , V_A and V_X for $V = W^\pm$ and Z , which carry the same properties as the SM W^\pm and Z bosons. We then make a field redefinition $V = V_T + V_0 + V_A + V_X$. The V_λ inherit all interactions of the W and Z ; redundant operators, e.g., $\Delta\mathcal{L} = M_Z^2 Z_T^\mu Z_{A\mu}$, are removed.

We extract QCD renormalization and R_2 counter terms (CTs) up to the first order in α_s

¹This is often through an interface to cross-platform Universal FeynRules Object (UFO) libraries [53–56].

using `FeynRules` (v2.3.36) with `NLOCT` (1.02) [57] and `FeynArts` (v3.11) [60]. At this point, the V_λ still have the same propagators as V and subsequently inherit all the CTs associated with V due to the $V = V_T + V_0 + V_A + V_X$ redefinitions. Importantly, the CTs here are purely QCD CTs at $\mathcal{O}(\alpha_s)$, not mixed QCD \otimes EW CTs. This means that our CTs do not depend on the helicity of V . While the $gg \rightarrow e^+e^-\mu^+\mu^-$ process at LO contains no UV divergencies, R_2 terms are present.

We then package all Feynman rules into a single set of software libraries². It is at this point that we modify the propagator library so that the “new” particles have propagators given by Eq. (5). Explicitly, V_T carries summed $\lambda = \pm 1$ polarizations and V_0 (V_A) carries the $\lambda = 0$ (A) polarization. W_X and Z_X , which are not used in the study, are copies of the unpolarized SM W and Z that we included for diagnostic purposes / closure tests.

We use the new UFO (`SM.Loop.VPolar`) in conjunction with `MadGraph5_aMC@NLO` (`mg5amc`) (v3.4.0) [59, 61, 62] to build the polarized matrix element, and hence compute the polarized cross section, for the full, loop-induced $2 \rightarrow 4$ process $gg \rightarrow e^+e^-\mu^+\mu^-$ at LO, i.e., at $\mathcal{O}(\alpha_s\alpha^2)$. We include the full dependence of the top quark [62]. We do not impose the NWA but remove all diagrams with photons; we justify removing photons in the next section. This level of diagram removal is a built-in ability `mg5amc` [61, 62]. For unpolarized propagators, we obtain 16 diagrams mediated by top triangles and top boxes, including diagrams with an internal Higgs, and obtain 14 diagrams each for massless u - and d -quark loops.

According to our method, all intermediate Z subgraphs, including non-resonant subgraphs, are split into “polarized” subgraphs. (For multiboson processes, this can generate a large diagram multiplicity.) For the doubly polarized matrix elements $(\lambda_1, \lambda_2) = (0, 0)$ and (T, T) , we remove all diagrams containing undesired V_λ . Again, this type of diagram removal is a built-in option in `mg5amc`. In both cases, we obtain 16 (14) diagrams when the top quark (a light quark) runs in the loop.

For the mixed polarized channel $(\lambda_1, \lambda_2) = (0, T) + (T, 0)$, we exploit the topology, coupling order, absence of photons. These conditions dictate that two exactly Z_λ propagators must appear in the full $2 \rightarrow 6$ process. We employ a type diagram filtering accept/reject diagrams³. For diagrams in-

duced by triangle loops, we require that exactly one Z_0 and one Z_T appear in any multi-vertex, tree subgraph attached to the loop. For diagrams induced by boxes, we require that one of the tree subgraphs attached to the loop contains Z_0 and another contains Z_T . We generate the expected 32 (28) diagrams for top (light) quark loops.

The matrix element for our closure test is obtained by removing all diagrams with photons and the auxiliary “ Z_X ” state. We otherwise keep all diagrams with $Z_\lambda \in \{Z_T, Z_0, Z_A\}$. For top quark diagrams, this generates $16 \times 3^2 = 144$ individual diagrams while $14 \times 3^2 = 126$ diagrams are generated for loops with light quarks.

Investigating polarization rates in loop-induced triple or quadruple boson production is outside the scope of this work. However, we have checked that the correct number of diagrams are generated for $gg \rightarrow Z_{\lambda_1}Z_{\lambda_2}Z_{\lambda_3} \rightarrow e^+e^-\mu^+\mu^-\tau^+\tau^-$. For the unpolarized case and assuming a massless tau, we obtain 228 (186) resonant and non-resonant diagrams for top (light) quark loops, and which includes 6 diagrams with four intermediate Z bosons. We obtain the same number of diagrams for the triple polarization configuration $(\lambda_1, \lambda_2, \lambda_3) = (0, 0, 0)$. When all polarizations are allowed, $\lambda_k \in \{0, T, A\}$, we obtain $n_{\text{top}} = (228 - 6) \times 3^3 + (6) \times 3^4 = 6480$ diagrams with a top quark loop, and $n_{\text{light}} = (186 - 6) \times 3^3 + (6) \times 3^4 = 5346$ diagrams for each light quark in the loop.

3. Polarized $Z_\lambda Z_{\lambda'}$ from gluon fusion

As a first demonstration of our method we present total and differential predictions for polarized $Z_\lambda Z_{\lambda'}$ production from ggF. We construct our matrix elements and simulate our signal processes at LO with `mg5amc` as described in Sec. 2.1. We use the `NNPDF31+LUXqed` NLO parton distribution function (PDF) (`lhaid=324900`) [63–65]. DGLAP evolution and PDF uncertainty extraction are handled by `LHAPDF` (v6.3.0) [66]. Further simulation details are given in [Appendix C](#).

3.1. Polarized cross sections in proton collisions

In Fig. 1 (top panel) we show the hadron-level cross section [fb] as a function of collider energy \sqrt{s} [TeV] for the full loop-induced, $2 \rightarrow 4$ process

$$gg \rightarrow Z_\lambda Z_{\lambda'} \rightarrow e^+e^-\mu^+\mu^- \quad (11)$$

at LO for unpolarized ZZ pairs (black band) as well as polarized $Z_T Z_T$ (blue band), $Z_T Z_0$ (purple band), and $Z_0 Z_0$ (green band) pairs. The $Z_T Z_0$ rate includes both $(T, 0)$ and $(0, T)$ helicity configurations. Helicity is defined in the (gg) frame. The unpolarized prediction does not employ the

²Our public `FeynRules` UFO entitled `SM.Loop.VPolar` is available from feynrules.irmp.ucl.ac.be/wiki/VPolarization

³Removing loop-level diagrams in `mg5amc` is a highly nontrivial issue. Our routine as implemented in `mg5amc` is available from the repository gitlab.cern.ch/riruiz/public-projects/-/tree/master/VPolar_ggZZ.

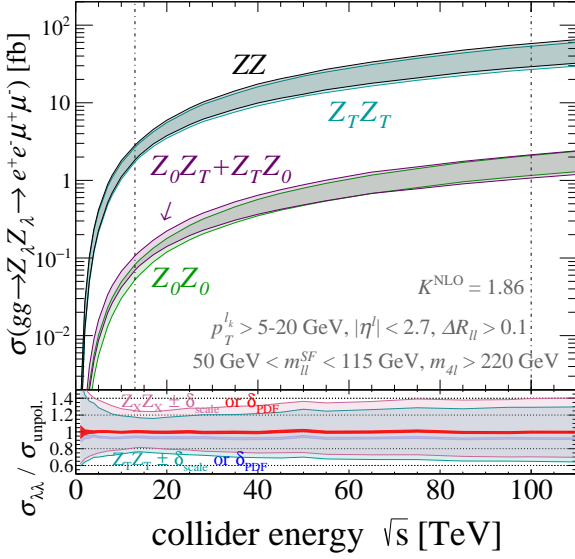


Figure 1: Upper panel: As a function of \sqrt{s} , the unpolarized $gg \rightarrow ZZ \rightarrow e^+ e^- \mu^+ \mu^-$ cross section (black band) with phase space cuts of Eq. (12), along with the analogous $Z_T Z_T$ (blue), $Z_T Z_0$ (purple), and $Z_0 Z_0$ (green) rates. Band thickness denotes the scale uncertainty. Lower panel: The ratio of the $Z_T Z_T$ (blue) and $Z_X Z_X$ (red) cross sections and their uncertainties relative to the unpolarized rate. (Z_X is the sum of the Z_T , Z_0 , and Z_A channels at the amplitude level.) Larger (transparent) bands are the scale uncertainties; smaller (solid) bands are the PDF uncertainties.

methodology of Sec. 2 and serves as a check. Band thickness corresponds to the scale uncertainty.

We remove photon diagrams, which are less important around the Z resonance, to make the relative importance of individual polarization configurations clearer. We also impose the following phase space cuts on the charged leptons:

$$p_T^{\ell_1(2)(3)(4)} > 20 \text{ (15) [10] \{5\}} \text{ GeV}, \quad (12a)$$

$$m_{4\ell} > 220 \text{ GeV}, \quad |\eta^\ell| < 2.7, \quad \Delta R_{\ell\ell} > 0.1 \quad (12b)$$

$$50 \text{ GeV} < m_{\ell\ell}^{\text{SF}} < 115 \text{ GeV}, \quad (12c)$$

where SF denotes same-flavor lepton pairs and charged leptons are ranked by p_T , i.e., $p_T^i > p_T^{i+1}$. These generator cuts reflect selection cuts that would be imposed in a real analysis in ATLAS or CMS. For all polarization channels and collider energies, we estimate⁴ missing QCD corrections

⁴Ref. [67] reports an NLO K -factor of $K^{\text{NLO}} \approx 1.53$ when using a (N)LO PDF with $\alpha_s(M_Z) \approx 0.130$ (0.118) for the (N)LO computation. To account for this, we reweight K^{NLO} by $(\alpha_s^{1\text{-loop}}/\alpha_s^{2\text{-loop}})^2 \approx 1.21$. We neglect the additional impact due to the different choices of μ_f, μ_r here and in Ref. [67], which should be small given their similarity.

by applying a constant K -factor of [67, 68]

$$K^{\text{NLO}} = 1.86. \quad (13)$$

Over the range $\sqrt{s} = 1 - 100$ TeV, the fiducial cross sections and relative scale uncertainties for various polarization configurations roughly span

$$\sigma_{ZZ, Z_T Z_T} \sim 10^{-2} \text{ fb} - 40 \text{ fb}, \quad (14a)$$

$$\sigma_{Z_T Z_0} \sim 10^{-3} \text{ fb} - 2 \text{ fb}, \quad (14b)$$

$$\sigma_{Z_0 Z_0} \sim 10^{-3} \text{ fb} - 2 \text{ fb}, \quad (14c)$$

$$\delta\sigma^{\text{scale}}/\sigma \Big|_{ZZ, Z_\lambda Z_{\lambda'}} \sim \pm 25\% - \pm 30\%. \quad (14d)$$

We do not show rates with the auxiliary polarization $\lambda = A$ since their contraction with currents containing massless leptons vanishes by the Dirac equation. For lower collider energies, we observe that the $(0, 0)$ rate is comparable but still lower than the mixed $(0, T) + (T, 0)$ rate. At higher collider energies, however, this difference disappears.

For concreteness, the QCD-improved cross sections (first column), scale uncertainties [%] (second), and PDF uncertainties [%] (third) at the LHC's current energy of $\sqrt{s} = 13$ TeV are

$$\sigma_{ZZ} \times K^{\text{NLO}} = 2.27 \text{ fb} \begin{matrix} +25\% & +1\% \\ -19\% & -1\% \end{matrix}, \quad (15a)$$

$$\sigma_{Z_T Z_T} \times K^{\text{NLO}} = 2.13 \text{ fb} \begin{matrix} +25\% & +1\% \\ -19\% & -1\% \end{matrix}, \quad (15b)$$

$$\sigma_{Z_0 Z_0} \times K^{\text{NLO}} = 85.9 \times 10^{-3} \text{ fb} \begin{matrix} +25\% & +1\% \\ -19\% & -1\% \end{matrix}, \quad (15c)$$

$$\sigma_{Z_0 Z_0} \times K^{\text{NLO}} = 65.1 \times 10^{-3} \text{ fb} \begin{matrix} +26\% & +1\% \\ -20\% & -1\% \end{matrix}, \quad (15d)$$

$$\sigma_{Z_X Z_X} \times K^{\text{NLO}} = 2.27 \text{ fb} \begin{matrix} +25\% & +1\% \\ -19\% & -1\% \end{matrix}. \quad (15e)$$

Here and below, Z_X denotes the sum over Z_T , Z_0 , and Z_A channels at the amplitude level and shows that the unpolarized rate is recovered. By closure, the interference is $\delta\sigma = \sigma_{ZZ} - \sum_{\lambda\lambda'} \sigma_{\lambda\lambda'} \sim \mathcal{O}(+1)$ ab, which is below our MC statistical uncertainty for 400k events. In terms of polarization fractions

$$f_{\lambda\lambda} \equiv \frac{\sigma_{Z_\lambda Z_\lambda}}{\sigma_{ZZ}} = \frac{\sigma_{Z_\lambda Z_\lambda}}{\sum_{\kappa\kappa'} \sigma_{Z_\kappa Z_{\kappa'}}}, \quad (16)$$

the LO predictions for various channels are:

$$f_{TT} = 93.3\%, \quad f_{00} = 2.9\%, \\ f_{T0+0T} = 3.8\%. \quad (17)$$

This is consistent with the results of Ref. [34].

In the lower panel of Fig. 1 we show the ratio of polarized (fiducial) cross sections $\sigma_{\lambda\lambda}$, along with their uncertainties relative to the central unpolarized ZZ rate. The larger (transparent) bands are the scale uncertainties at LO and reach approximately $\delta\sigma_{\lambda\lambda}^{\text{scale}}/\sigma_{ZZ} \sim \pm 20\% - \pm 40\%$. The smaller

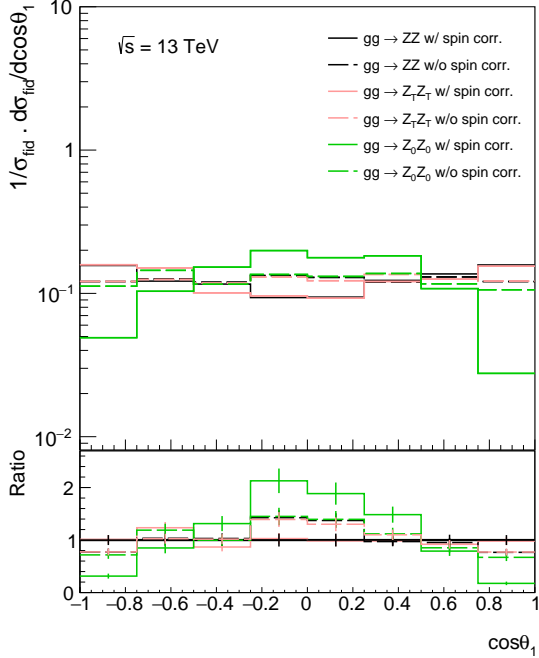


Figure 2: Comparison between simulated polarized $gg \rightarrow Z_\lambda Z_{\lambda'} \rightarrow e^+ e^- \mu^+ \mu^-$ events with phase space cuts of Eqs. (12) and (19), with and without spin correlation. The ratios are with respect to the unpolarized result with spin correlation.

(solid) bands are the PDF uncertainties and reach about $\delta\sigma_{\lambda\lambda}^{\text{PDF}}/\sigma_{ZZ} \lesssim \pm 1.5\%$ for $\sqrt{s} \gtrsim 5$ TeV. Specifically, we show the $Z_T Z_T$ ratio (blue bands), which sits uniformly at around $(\sigma_{TT}/\sigma_{ZZ}) \sim 90\% - 95\%$, and the rate of $Z_X Z_X$ (red bands) sits uniformly at unity. The $Z_X Z_X$ ratio serves as a closure test and check of our methodology.

3.2. Spin-correlation in polarized $gg \rightarrow ZZ \rightarrow 4\ell$

Measurements of ZZ polarization in ggF processes require public MC generators matched to parton showers that can simultaneously model loop-induced processes, helicity-polarized intermediate states, and still preserve spin correlation.

Spin correlations are essential for the observables used in a typical 4ℓ -analyses. For example: matrix-element discriminants rely on spin correlations between final-state leptons to separate signal processes from irreducible background [69–71].

As another demonstration of our method, Fig. 2 shows a comparison between simulations of the $gg \rightarrow ZZ \rightarrow 4\ell$ process with and without spin correlation. The variable θ_1 is the angle between the three-momentum of V_2 and the three-momentum of the hardest fermion in the decay of V_1 , ℓ_{11} , in

the rest-frame of V_1 , where V_1 is the same-flavor $\ell^+ \ell^-$ pair whose mass is closest to M_Z .

The $\cos\theta_1$ distribution captures the spin correlation in the process that enters the matrix-element discriminants used in Higgs analyses. A recent measurement by the ATLAS collaboration of polarization states in $q\bar{q} \rightarrow ZZ \rightarrow 4\ell$ uses a reweighting based on this variable to approximate the effect of polarization in $gg \rightarrow ZZ \rightarrow 4\ell$ [72]. The comparison shows how acceptance estimates would be incorrect if spin correlations were ignored. The largest acceptance difference is observed in $Z_0 Z_0$ production (green), with smaller effects in $Z_T Z_T$ (red). We note the importance of spin correlation in ggF already at lowest order.

4. Sensitivity to longitudinally polarized diboson pairs from gluon fusion

We now present our projections for extracting polarization cross sections from LHC collisions.

4.1. Template method for extracting polarization

We continue our focus on $Z_\lambda Z_{\lambda'}$ production. Specifically, we consider two signal processes

$$\text{ggF} : pp \xrightarrow{gg} Z_\lambda Z_{\lambda'} \rightarrow e^+ e^- \mu^+ \mu^- , \quad (18a)$$

$$\text{EW} : pp \xrightarrow{qq} Z_\lambda Z_{\lambda'} jj \rightarrow e^+ e^- \mu^+ \mu^- jj , \quad (18b)$$

at $\mathcal{O}(\alpha^4 \alpha_s^2)$ and $\mathcal{O}(\alpha^6)$. The ggF channel employs the method of Sec. 2 while the EW channel, which includes both VBF and quark-annihilation topologies, employs the truncated-propagator method implemented in Ref. [46]. We also consider the (irreducible) unpolarized background at $\mathcal{O}(\alpha^4)$

$$\text{diboson} : pp \xrightarrow{q\bar{q}} ZZ \rightarrow e^+ e^- \mu^+ \mu^- , \quad (18c)$$

which we generate at NLO with Sherpa (v2.2) [73].

We employ the so-called template method, where signal processes are treated as linear combinations of sub-processes, or templates, with unknown weights and fit these weights to (simulated) data. By using individual $Z_\lambda Z_{\lambda'}$ helicity configurations as our templates, we can identify the unknown weights as the polarization fractions $f_{\lambda\lambda'}$.

We choose the following polarization configurations as our basis of templates: (i) $Z_0 Z_0$, (ii) $Z_T Z_T$, and (iii) $Z_T Z_0$. This last one is defined by subtracting the $Z_0 Z_0$ and $Z_T Z_T$ channels from the unpolarized process. Formally, the $Z_T Z_0$ template includes a contribution from interference but this is estimated to be small by our closure test. Formally, the $Z_T Z_0$ template includes the Z_A component and interference. For resonant diagrams, the Z_A contribution is zero because we assume final-state charged leptons are massless. For simplicity,

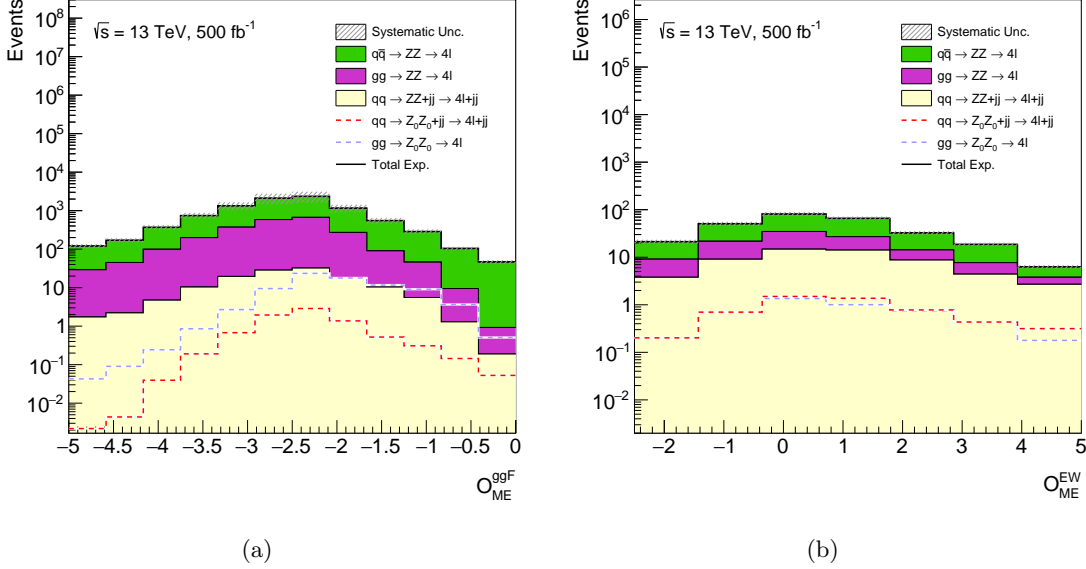


Figure 3: Templates for the observables used in the (a) ggF and (b) EW regions as defined in Eq. (22). Templates are stacked and normalized to $\mathcal{L} = 500 \text{ fb}^{-1}$ of integrated luminosity in $\sqrt{s} = 13 \text{ TeV}$ LHC collisions. Contributions from longitudinally polarized $Z_0 Z_0$ pairs in ggF (blue dash) and EW (red dash) production modes are overlaid. The black solid line indicates the total expected (Total Exp.) number of events with acceptance effects from selection criteria but without taking into account detection efficiency. The hatched band is an estimate of modeling and experimental uncertainties.

we will keep the notation $Z_T Z_0$ for all these contributions hereafter. To maximize the sensitivity to longitudinally polarized $Z_0 Z_0$ pairs, events are divided into two categories, called “ggF” and “EW”, according to the selection criteria below.

4.2. Event selection and observable definitions

Simulated events are selected using criteria similar to the $H^{(*)} \rightarrow ZZ \rightarrow 4\ell$ analyses performed by ATLAS and CMS [69, 71, 74, 75]. Specifically, we require signal and background processes to satisfy the selection cuts given in Eq. (12) but tighten the $m_{\ell\ell}^{\text{SF}}$ requirement such that

$$50 \text{ GeV} < m_{\ell_1 \ell_2}^{\text{SF}} < 106 \text{ GeV} , \quad (19)$$

where $(\ell_1 \ell_2)$ is the same-flavor pair with mass closest to M_Z . Jets are reconstructed by clustering all final-state hadrons and photons using the anti- k_t algorithm [76] with a radius parameter of $R = 0.4$. Jet candidates are required to satisfy

$$p_T^j > 30 \text{ GeV} \text{ and } |\eta^j| < 4.4 . \quad (20)$$

Jets that overlap with any signal lepton are discarded. To increase sensitivity to the EW mode, EW events are required to additionally satisfy

$$n_j \geq 2, \quad |\Delta\eta(j_1, j_2)| > 3, \quad |\cos\theta_1| < 0.7 . \quad (21)$$

All other events are assigned to the ggF region.

For both regions, templates are built using the matrix-element (ME) kinematic discriminants

$$O_{\text{ME}}^{\text{ggF}} = \log_{10} \left(\frac{|\text{ME}_{ggZ_0Z_0}|^2}{|\text{ME}_{ggZ_TZ_T}|^2 + 0.1 \cdot |\text{ME}_{q\bar{q}ZZ}|^2} \right) , \quad (22a)$$

$$O_{\text{ME}}^{\text{EW}} = \log_{10} \left(\frac{|\text{ME}_{qqZ_0Z_0jj}|^2}{|\text{ME}_{qqZ_TZ_Tjj}|^2} \right) . \quad (22b)$$

The templates for the ggF and EW regions are shown in Figs. 3a and 3b, respectively.

4.3. Statistical model and expected sensitivity

Expected sensitivity is assessed for two integrated luminosity scenarios at $\sqrt{s} = 13 \text{ TeV}$: $\mathcal{L} = 500$ and $\mathcal{L} = 3000 \text{ fb}^{-1}$. The first scenario provides a good approximation for an analysis using the full Run 2 and Run 3 data sets of the LHC. The latter corresponds to the full HL-LHC program.

The expected sensitivity is probed by a profile log-likelihood ratio test statistic [77]. The likelihood is built from the product of Poisson probability densities over the bins shown in Fig. 3a and 3b, and Gaussian constraint terms to represent systematic uncertainties with nuisance pa-

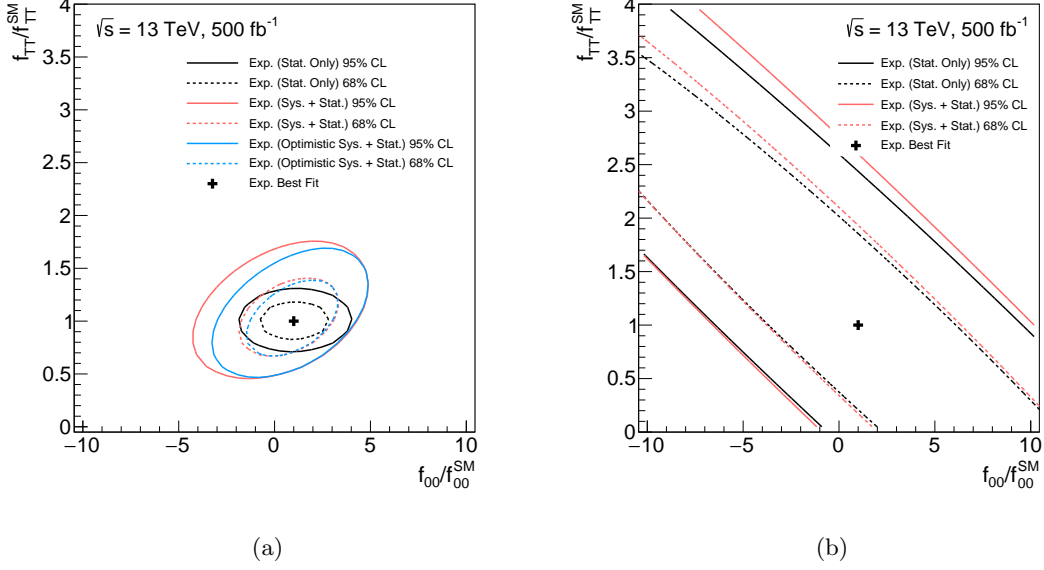


Figure 4: Test statistic 2D scan of helicity fractions normalized to SM predictions of $Z_\lambda Z_{\lambda'}$ in (a) $gg \rightarrow Z_\lambda Z_{\lambda'} \rightarrow 4\ell$ and (b) EW $qq \rightarrow Z_\lambda Z_{\lambda'} jj \rightarrow 4\ell jj$, assuming $\mathcal{L} = 500 \text{ fb}^{-1}$ of LHC data.

rameters (NP) α . This profile is given by

$$\lambda(\mu_{00}^{\text{ggF}}, \mu_{00}^{\text{ggF}}, \alpha) = \prod_{i \in \text{bins}} \text{Pois} \left[N(1, 1) | N(\mu_{00}^{\text{ggF}}, \mu_{00}^{\text{EW}}) \right] \times \prod_{\alpha \in \text{NP}} \text{Gaus}(\alpha/\sigma_\alpha | 0, 1), \quad (23)$$

where σ_α is the uncertainty associated with α .

We consider three uncorrelated sources of systematic uncertainties: a 10% experimental uncertainty on all processes, a 25% modeling uncertainty on ggF, and a 5% modeling uncertainty on all other processes. We also consider the optimistic scenario where ggF modeling uncertainties are reduced to 15% [29]. The function $N(\mu_{00}^{\text{ggF}}, \mu_{00}^{\text{EW}})$ is the number of $ZZ \rightarrow 4\ell$ events and is given by the sum of individual channels ($N^k = \mathcal{L} \times \sigma^k$):

$$N(\mu_{00}^{\text{ggF}}, \mu_{00}^{\text{EW}}) = N^{q\bar{q}ZZ} + N^{ggZ_T Z_T} + N^{ggZ_T Z_0} + \mu_{00}^{\text{ggF}} N^{ggZ_0 Z_0} + N^{qqZ_T Z_T jj} + N^{qqZ_T Z_0 jj} + \mu_{00}^{\text{EW}} N^{qqZ_0 Z_0 jj}. \quad (24)$$

Here, μ_{00}^{ggF} and μ_{00}^{EW} are signal strengths and multiply the SM predictions for $gg \rightarrow Z_0 Z_0 \rightarrow 4\ell$ and EW $qq \rightarrow Z_0 Z_0 qq \rightarrow 4\ell qq$, respectively. The μ_{00} are varied to maximize the log-likelihood function; other polarization components remain unchanged. We further take the natural logarithm of the likelihood and multiply by -2 (2NLL) to obtain a χ^2 asymptotic distribution. The test statistic 2NLL

is obtained by profiling the NPs and any signal strength not being inferred.

With the HL-LHC, ATLAS and CMS can constrain the production of $gg \rightarrow Z_0 Z_0 \rightarrow 4\ell$ ($qq \rightarrow Z_0 Z_0 qq \rightarrow 4\ell qq$) to within $2.5 \times$ ($4.5 \times$) the SM prediction. The expected significance for observing $gg \rightarrow Z_0 Z_0 \rightarrow 4\ell$ is 1.3σ with $\mathcal{L} = 3000 \text{ fb}^{-1}$, which is comparable to the expected sensitivity for $qq \rightarrow Z_0 Z_0 jj \rightarrow 4\ell jj$ assessed in Ref. [78]. The corresponding reach at Run 3 is $4 \times$ ($8 \times$) the SM prediction. By multiplying by the ratio $\sigma_{00}/\sigma_{\text{unpol}}$ with respect to the unpolarized cross-section, limits on μ_{00} can be translated into limits on the polarization fraction f_{00} .

To extract the helicity fractions of $Z_\lambda Z_{\lambda'}$ pairs $f_{\lambda\lambda'}$ (relative to the SM prediction $f_{\lambda\lambda'}^{\text{SM}}$) we again use the template method. We impose the normalization $f_{00} + f_{TT} + f_{T0+0T+\text{int.}} = 1$, where $f_{T0+0T+\text{int.}}$ accounts for both the $(0, T) + (0, T)$ polarization configurations and interference. This reduces the number of independent helicity parameters in the fit to only two: one for the longitudinal fraction ($f_{00}/f_{00}^{\text{SM}}$) and the other for the transverse fraction ($f_{TT}/f_{TT}^{\text{SM}}$). Two statistical models are built to probe the ggF and EW channels individually.

The model for the ggF process is given by

$$\begin{aligned}
N\left(\frac{f_{00}}{f_{00}^{\text{SM}}}, \frac{f_{TT}}{f_{TT}^{\text{SM}}}\right) &= N^{q\bar{q}ZZ} + N^{qqZZjj} \\
&+ \left(\frac{f_{00}}{f_{00}^{\text{SM}}}\right) \cdot N^{ggZ_0Z_0} + \left(\frac{f_{TT}}{f_{TT}^{\text{SM}}}\right) \cdot N^{ggZ_TZ_T} \\
&+ \frac{s - \frac{f_{00}}{f_{00}^{\text{SM}}} \cdot s_{00} - \frac{f_{TT}}{f_{TT}^{\text{SM}}} \cdot s_{TT}}{s_{T0}} \cdot N^{ggZ_TZ_0}. \quad (25)
\end{aligned}$$

Here, s , s_{00} , s_{TT} and s_{T0} are the integrals over the templates of the fiducial, longitudinal and transverse polarizations in both the ggF and EW regions. The expected sensitivity for measuring the values of $f_{00}/f_{00}^{\text{SM}}$ and $f_{TT}/f_{TT}^{\text{SM}}$ in ggF and EW events is shown in Figs. 4a and 4b, respectively. We anticipate that projected sensitivities could be improved by employing more sophisticated analysis techniques, e.g., deep neural networks, that are common in ATLAS and CMS frameworks.

5. Measuring Quantum Properties

Spin, and hence spin-correlation in production and decay chains of heavy particles, is a fundamental quantum property of elementary particles. With our methodology, we can additionally propose two further tests of quantum properties in multiboson systems at high energies: the existence of spin correlation and quantum entanglement.

To show the importance of spin correlation in $Z_\lambda Z_{\lambda'}$ production, we build a statistical model that assesses the sensitivity of the LHC data to spin-correlation following Ref. [79]. The model

$$\begin{aligned}
N(f) &= N^{q\bar{q}ZZ} + N^{qqZZjj} \\
&+ f \cdot N_{\text{SM}}^{ggZZ} + (1-f) \cdot N_{\text{uncorr}}^{ggZZ} \quad (26)
\end{aligned}$$

describes the number of $ZZ \rightarrow 4\ell$ events (N) as a combination of the $gg \rightarrow ZZ \rightarrow 4\ell$ process with and without spin correlation, parameterized by f .

Inference on the parameter f , which represents the degree of observed spin correlation, is performed with the same test statistic from Eq. (23). Templates in $\cos\theta_1$, as shown in Fig. 2, are built for all processes. Fig. 5a shows that with Run 2 and 3 data alone, a 5σ exclusion of the null hypothesis (no correlation) may already be possible.

Recently, several groups have discussed the possibility of measuring quantum entanglement with $H \rightarrow VV$ [19–22, 80–82] and $t\bar{t}$ processes [18, 83] at the LHC. The ATLAS collaboration also recently published the first experimental result using $t\bar{t}$ events [84]. In Ref. [20], the authors showed that the absence of quantum entanglement in $H \rightarrow VV$ decays is equivalent to testing the hypothesis that

only the $H \rightarrow V_0V_0$ polarization configuration occurs in nature. As models testing quantum entanglement are similar to those testing polarization and spin correlation, our methodology is applicable. Specifically, our Feynman rules can be used to compute off-shell Higgs production with four final-state fermions when one or both intermediate weak bosons are polarized.

Here we show the LHC is able to falsify the (null) hypothesis that there is no entanglement in $H \rightarrow VV$ splittings and hence no $gg \rightarrow H^* \rightarrow Z_T Z_T \rightarrow 4\ell$ subprocess, in the high-mass region where the Higgs boson is produced off-shell. We extend the statistical model of Eq. (24) to describe separately the contribution of diagrams with an s -channel Higgs boson (S), the contribution from non-Higgs, “box” diagrams (B), and the interference (I) between them. The method described in Sec. 2 is also employed for these additional templates. The interference template is defined by subtracting the signal and background processes from the full process. This is given by

$$\begin{aligned}
N(\mu_{TT}^{\text{Higgs}}) &= N^{q\bar{q}ZZ} + N^{qqZZjj} \\
&+ N^{ggZ_0Z_0} + N^{ggZ_TZ_0} + N_B^{ggZ_TZ_T} \quad (27) \\
&+ \mu_{TT}^{\text{Higgs}} N_S^{ggZ_TZ_T} + \sqrt{\mu_{TT}^{\text{Higgs}}} N_I^{ggZ_TZ_T}.
\end{aligned}$$

The signal strength μ_{TT}^{Higgs} is the cross section for $Z_T Z_T$ pairs normalized to the SM prediction.

The expected sensitivity is assessed by using templates of the observable $O_{\text{ME}}^{\text{ggF}}$ defined in Eq. (22a). For Runs 2 and 3, Fig. 5b shows that the no entanglement hypothesis ($\mu_{TT}^{\text{Higgs}} = 0$) can be rejected with approximately 2σ significance. An even stronger rejection can be obtained by optimizing the observable for Higgs processes.

6. Summary and Conclusion

In this work we proposed a method for computing polarized cross sections that works at the level of Feynman rules. Previous methods typically work at the amplitude or squared-amplitude levels and require specialized event generators. As illustrated in Eqs. (6)-(7), the basic idea is to identify the sum over polarizations in a single (unpolarized) propagator subgraph as the sum over multiple (polarized) propagator subgraphs. Our method’s efficient implementation into existing, public simulation tools enables realistic simulations of tree- and loop-induced processes, including $gg \rightarrow V_\lambda V_{\lambda'} \rightarrow 4\ell, 2\ell 2\nu$ while maintaining spin correlation, off-shell effects, as well as interference between resonant and non-resonant diagrams.

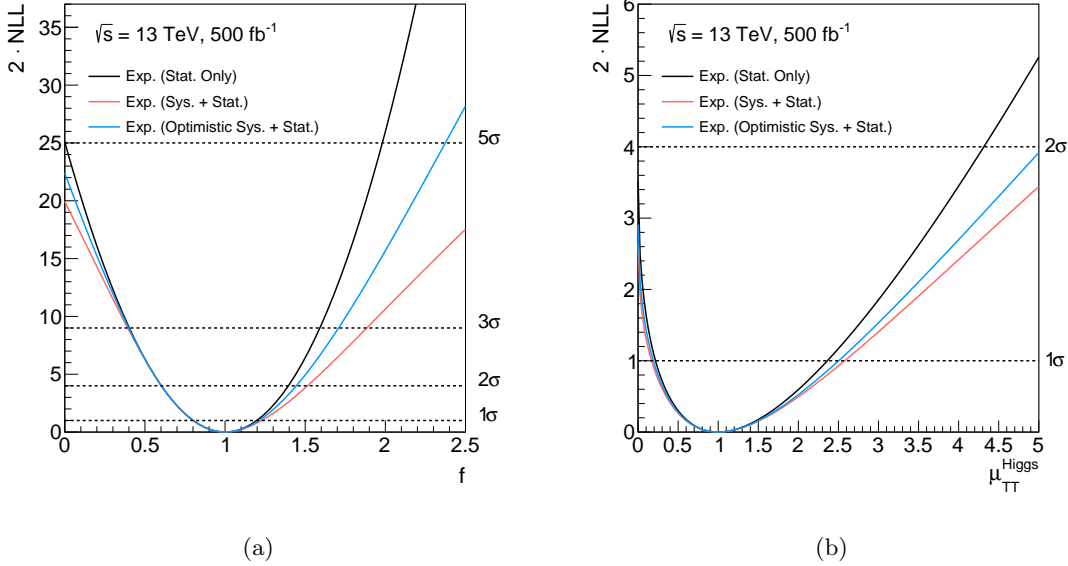


Figure 5: (a) Test statistics scan with respect to the parameter f which represents the degree of spin-correlation in $gg \rightarrow ZZ \rightarrow 4\ell$ process, assuming $\mathcal{L} = 500 \text{ fb}^{-1}$ of LHC data. (b) Same as (a) but with respect to signal strength multiplying the SM production of polarized $gg \rightarrow H^* \rightarrow Z_T Z_T \rightarrow 4\ell$.

After exploring some phenomenological predictions for polarized $Z_\lambda Z_{\lambda'}$ pairs, we presented sensitivity projections for measuring polarized $Z_\lambda Z_{\lambda'}$ pairs when produced via gluon fusion and EW processes during Run 2 and Run 3 of the LHC, and for the larger HL-LHC dataset. We also presented prospects for measuring quantum properties, e.g., entanglement in multiboson systems.

We believe that the techniques describe in this work can be used by experimental collaborations to further explore the production of Higgs bosons at high virtuality and by the theory community to explore ramifications for new physics. While we have focused only on a SM case study, the basic idea can be applied to resonances in new physics scenarios as well as to weak bosons and the top quark in the Standard Model Effective Field Theory. Finally, there are field-theoretic aspects of “polarization as a Feynman rule” that merit further investigation and we encourage such studies.

Acknowledgements

RR thanks the CalTech theory group for hosting him while this work was completed. The authors also thank Benjamin Fuks, Verena Martinez, Olivier Windu Mattelaer, and Giovanni Pelliccioli for useful discussions.

The work of MJ, RCLSA, and JS is supported in part by the DOE grant DE-SC0010004. RR acknowledges the support of the Narodowe Centrum Nauki under Grants No. 2019/34/E/ST2/

00186 and No. 2023/49/B/ST2/04330 (SNAIL). The author also acknowledges the support of the Polska Akademia Nauk (grant agreement PAN.BFD.S.BDN.613.022.2021 - PASIFIC 1, POPSICLE). This work has received funding from the European Union’s Horizon 2020 research and innovation program under the Skłodowska-Curie grant agreement No. 847639, and from the Polish Ministry of Education and Science. The authors would like to acknowledge the contribution of the COST Action CA22130 (COMETA).

Appendix A. Implementation details

For the transverse and longitudinal polarization vectors, we adopt the HELAS convention [58]. For the auxiliary polarization vector, we follow Ref. [46] and use

$$\varepsilon^\mu(q, \lambda = A) = \frac{q^\mu}{M_V} \sqrt{\frac{q^2 - M_V^2}{M_V^2}}. \quad (\text{A.1})$$

To implement the methodology described in Sec. 2, we start from the full `FeynRules` SM model file `sm.fr` [53–56] and introduce the particles

$$Z : ZX, Z0, ZT, ZA, \quad (\text{A.2a})$$

$$W^+ : WX+, W0+, WT+, WA+, \quad (\text{A.2b})$$

$$W^- : WX-, W0-, WT-, WA-, \quad (\text{A.2c})$$

by making several copies of `V[n]` objects. We ensure that the appropriate values and classifications

for internal/external parameters are inherited. We then make the field (re)definition

```
...
Definitions ->
  {Z[mu_] -> Z0[mu] + ZT[mu] + ZA[mu] + ZX[mu]}
...
```

```
Definitions ->
  {W[mu_] -> W0[mu] + WT[mu] + WA[mu] + WX[mu]}
```

and remove new but unphysical two-point vertices. We also (re)assign the following PIDs:

$$Z(239), W^\pm(\pm 249), \quad (\text{A.3a})$$

$$Z_X(23), W_X^\pm(\pm 24), \quad (\text{A.3b})$$

$$Z_0(230), W_0^\pm(\pm 240), \quad (\text{A.3c})$$

$$Z_T(231), W_T^\pm(\pm 241), \quad (\text{A.3d})$$

$$Z_A(232), W_A^\pm(\pm 242). \quad (\text{A.3e})$$

The fields $Z(239)$ and $W^\pm(\pm 249)$ are designated `Unphysical->True`, meaning that they do not appear in the final UFO library. Importantly, a feature in `mg5amc` is to override particles labels when PIDs match those of SM particles. This means that in `mg5amc`, the unpolarized fields $Z_X(23)$ and $W_X^\pm(\pm 24)$ are *automatically* relabeled `z`, `w+`/`w-`.

We extract QCD renormalization and R_2 counter terms up to the first order in α_s using `FeynRules` (v2.3.36) with `NLOCT` (1.02) [57] and `FeynArts` (v3.11) [60], and package them into the `SM_Loop_VPolar` UFO, which is publicly available from feynrules.irmp.ucl.ac.be/wiki/VPolarization. Finally, we modify (by hand) the `particles.py` file so that the “new” particles have propagators given by

$$\text{VX} : \Pi_{\mu\nu}^{\text{VX}} = \sum_{\lambda \in \{\pm 1, 0, A\}} \Pi_{\mu\nu}^{\text{V}\lambda}, \quad (\text{A.4a})$$

$$\text{V0} : \Pi_{\mu\nu}^{\text{V0}} = \sum_{\lambda \in \{\pm 1\}} \Pi_{\mu\nu}^{\text{V}\lambda}, \quad (\text{A.4b})$$

$$\text{VT} : \Pi_{\mu\nu}^{\text{VT}} = \Pi_{\mu\nu}^{\text{V}\lambda=0}, \quad (\text{A.4c})$$

$$\text{VA} : \Pi_{\mu\nu}^{\text{VA}} = \Pi_{\mu\nu}^{\text{V}\lambda=A}, \quad (\text{A.4d})$$

where $\Pi_{\mu\nu}^{\text{V}\lambda}$ is the truncated propagator in Eq. (5).

Appendix B. Test statistic scan for polarization extraction

Figure B.6 shows the expected sensitivity for the observation of longitudinally polarized $Z_0 Z_0$ pairs in (a,c) $gg \rightarrow ZZ \rightarrow 4\ell$ and (b,d) $qq \rightarrow ZZjj \rightarrow 4\ell jj$ production in the high-mass regime (a,b) after Runs 2 and 3 of LHC data taking, i.e., $\mathcal{L} = 500 \text{ fb}^{-1}$ at $\sqrt{s} = 13 \text{ TeV}$, as well as (c,d) with the full HL-LHC data set, i.e., $\mathcal{L} = 3000 \text{ fb}^{-1}$.

Appendix C. Computational Setup

We assume $n_f = 5$ massless quarks, with a Cabibbo-Kobayashi-Maskawa matrix equal to the identity matrix, i.e., no quark flavor mixing. Other SM inputs are set to the following values:

$$\begin{aligned} m_t(m_t) &= 173.3 \text{ GeV}, m_h = 125.7 \text{ GeV}, \\ M_Z &= 91.1876 \text{ GeV}, \alpha_{\text{QED}}^{-1}(M_Z) = 127.94, \\ G_F &= 1.174560 \cdot 10^{-5} \text{ GeV}^{-2}. \end{aligned} \quad (\text{C.1})$$

The central ($\zeta = 1$) collinear factorization and renormalization scales are set to be half the sum of the transverse energy of final-state particles (f):

$$\mu_f, \mu_r = \zeta \times \mu_0, \quad \mu_0 \equiv \sum_f \sqrt{m_f^2 + p_{Tf}^2}. \quad (\text{C.2})$$

Scale uncertainties are estimated by varying ζ discretely over the range $\{0.5, 1.0, 2.0\}$. For select processes, we include up to one additional parton in the matrix element using the multi-leg matching (MLM) [85, 86]. For MLM in the gluon fusion channel, diagrams in which neither a Z nor a H is attached to the quark loop are filtered out since they are part of the $q\bar{q}$ annihilation channel. Simulated events are showered and hadronized using `Pythia8` [87] (`tune=pp:14`) and matched to the `NNPDF23qed` LO PDF (PDF:`pSet=13`) [88]. Hadrons are clustered using `FastJet` [89, 90].

Using `SM_Loop_VPolar` in `MadGraph5_aMC@NLO` (`mg5amc`), loop-induced processes such as Eq. (11) can be simulated at lowest order and be passed to other programs for further processes, e.g., parton showering. For $gg \rightarrow Z_T Z_T \rightarrow e^+ e^- \mu^+ \mu^-$, the relevant `mg5amc` syntax to build matrix elements that includes spin-correlation, off-shell effects, and interference is:

```
import model SM_Loop_ZPolar
generate g g > e+ e- mu+ mu- QED=4 QCD=2
[noborn = QCD] / a z z0 za
output ZPolar_gg_eemm_TT_QED4_QCD2_XLO
```

The `g g > e+ e- mu+ mu-` syntax will interfere all instances of $Z_\lambda Z_{\lambda'}$. To filter out unwanted diagrams, including photon contributions, the “/ a z z0 za” syntax is added. The matrix elements for the analogous (i) $Z_0 Z_0$, (ii) $Z_A Z_A$, and (iii) $Z_X Z_X$ channels can be generated using the filters: (i) /a z z0 zt, (ii) / a z z0 zt, (iii) / a z. For the mixed-polarization configuration $Z_0 Z_T + Z_T Z_0$, we apply the diagram selection described in Sec. 2.1 and available from the repository given in Footnote 3. The relevant `mg5amc` syntax is then

```
generate g g > e+ e- mu+ mu- QED=4 QCD=2
[noborn = QCD] /
a --loop_filter=True
```

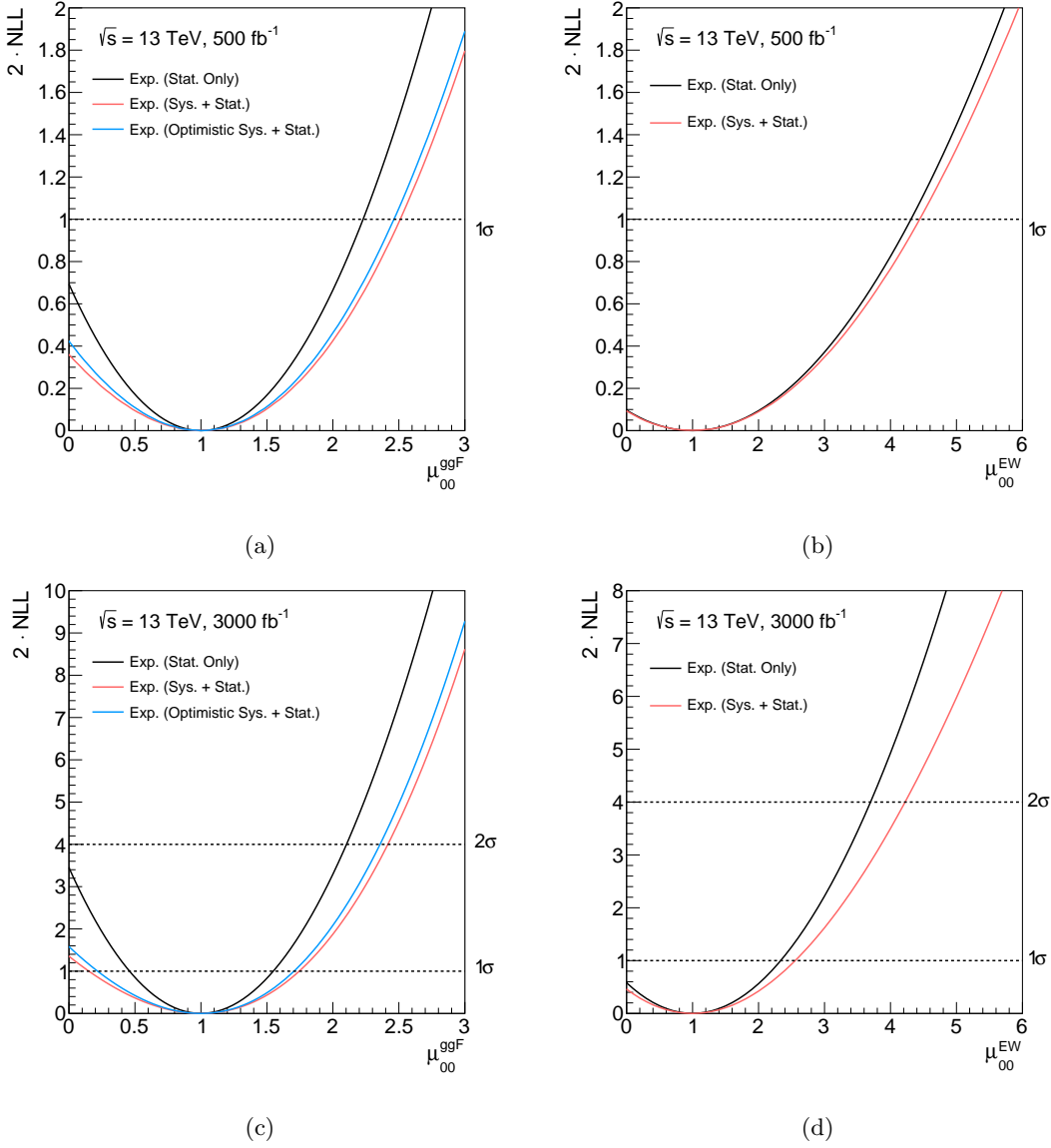


Figure B.6: Test statistic scan with respect to signal strength multiplying the SM production of polarized (a) $gg \rightarrow Z_0 Z_0 \rightarrow 4\ell$ and (b) $EW qq \rightarrow Z_0 Z_0 jj \rightarrow 4\ell jj$ assuming $\mathcal{L} = 500 \text{ fb}^{-1}$ of LHC data at $\sqrt{s} = 13 \text{ TeV}$. (c,d) Same as (a,b) but for $\mathcal{L} = 3000 \text{ fb}^{-1}$.

The cross sections in Eq. (15) can be obtained using the following (and similar) commands:

```

launch ZPolar_gg_eemm_00_QED4_QCD2_XL0
analysis=off
set pldlabel lhpdf
set lhaid 324900
set lhc 13
set nevents 4k
set dynamical_scale_choice 3
set me_frame [3,4,5,6]
set use_syst true
set no_parton_cut
set mml 50

```

```

set mmlmax 115
set mml 220
set etal 2.7
set drll 0.1
set ptl1min 20
set ptl2min 15
set ptl3min 10
set ptl4min 5
done

```

[1] J. C. Pati, A. Salam, Lepton Number as the Fourth Color, Phys. Rev. D 10 (1974) 275–289, [Erratum: Phys.Rev.D 11, 703–703 (1975)]. doi: [10.1103/PhysRevD.10.275](https://doi.org/10.1103/PhysRevD.10.275).

- [2] R. N. Mohapatra, J. C. Pati, Left-Right Gauge Symmetry and an Isoconjugate Model of CP Violation, *Phys. Rev. D* 11 (1975) 566–571. doi:[10.1103/PhysRevD.11.566](https://doi.org/10.1103/PhysRevD.11.566).
- [3] R. N. Mohapatra, J. C. Pati, A Natural Left-Right Symmetry, *Phys. Rev. D* 11 (1975) 2558. doi:[10.1103/PhysRevD.11.2558](https://doi.org/10.1103/PhysRevD.11.2558).
- [4] G. Senjanovic, R. N. Mohapatra, Exact Left-Right Symmetry and Spontaneous Violation of Parity, *Phys. Rev. D* 12 (1975) 1502. doi:[10.1103/PhysRevD.12.1502](https://doi.org/10.1103/PhysRevD.12.1502).
- [5] G. Senjanovic, Spontaneous Breakdown of Parity in a Class of Gauge Theories, *Nucl. Phys. B* 153 (1979) 334–364. doi:[10.1016/0550-3213\(79\)90604-7](https://doi.org/10.1016/0550-3213(79)90604-7).
- [6] D. B. Kaplan, H. Georgi, SU(2) x U(1) Breaking by Vacuum Misalignment, *Phys. Lett. B* 136 (1984) 183–186. doi:[10.1016/0370-2693\(84\)91177-8](https://doi.org/10.1016/0370-2693(84)91177-8).
- [7] D. B. Kaplan, H. Georgi, S. Dimopoulos, Composite Higgs Scalars, *Phys. Lett. B* 136 (1984) 187–190. doi:[10.1016/0370-2693\(84\)91178-X](https://doi.org/10.1016/0370-2693(84)91178-X).
- [8] H. Georgi, D. B. Kaplan, Composite Higgs and Custodial SU(2), *Phys. Lett. B* 145 (1984) 216–220. doi:[10.1016/0370-2693\(84\)90341-1](https://doi.org/10.1016/0370-2693(84)90341-1).
- [9] M. J. Dugan, H. Georgi, D. B. Kaplan, Anatomy of a Composite Higgs Model, *Nucl. Phys. B* 254 (1985) 299–326. doi:[10.1016/0550-3213\(85\)90221-4](https://doi.org/10.1016/0550-3213(85)90221-4).
- [10] R. Contino, Y. Nomura, A. Pomarol, Higgs as a holographic pseudoGoldstone boson, *Nucl. Phys. B* 671 (2003) 148–174. arXiv:[hep-ph/0306259](https://arxiv.org/abs/hep-ph/0306259), doi:[10.1016/j.nuclphysb.2003.08.027](https://doi.org/10.1016/j.nuclphysb.2003.08.027).
- [11] K. Agashe, R. Contino, A. Pomarol, The Minimal composite Higgs model, *Nucl. Phys. B* 719 (2005) 165–187. arXiv:[hep-ph/0412089](https://arxiv.org/abs/hep-ph/0412089), doi:[10.1016/j.nuclphysb.2005.04.035](https://doi.org/10.1016/j.nuclphysb.2005.04.035).
- [12] R. Contino, L. Da Rold, A. Pomarol, Light custodians in natural composite Higgs models, *Phys. Rev. D* 75 (2007) 055014. arXiv:[hep-ph/0612048](https://arxiv.org/abs/hep-ph/0612048), doi:[10.1103/PhysRevD.75.055014](https://doi.org/10.1103/PhysRevD.75.055014).
- [13] K. Agashe, R. Contino, L. Da Rold, A. Pomarol, A Custodial symmetry for $Zb\bar{b}$, *Phys. Lett. B* 641 (2006) 62–66. arXiv:[hep-ph/0605341](https://arxiv.org/abs/hep-ph/0605341), doi:[10.1016/j.physletb.2006.08.005](https://doi.org/10.1016/j.physletb.2006.08.005).
- [14] B. Bellazzini, C. Csáki, J. Serra, Composite Higgses, *Eur. Phys. J. C* 74 (5) (2014) 2766. arXiv:[1401.2457](https://arxiv.org/abs/1401.2457), doi:[10.1140/epjc/s10052-014-2766-x](https://doi.org/10.1140/epjc/s10052-014-2766-x).
- [15] G. Panico, A. Wulzer, *The Composite Nambu-Goldstone Higgs*, Vol. 913, Springer, 2016. arXiv:[1506.01961](https://arxiv.org/abs/1506.01961), doi:[10.1007/978-3-319-22617-0](https://doi.org/10.1007/978-3-319-22617-0).
- [16] A. I. Hernández-Juárez, G. Tavares-Velasco, A. Fernández-Télez, New evaluation of the HZZ coupling: Direct bounds on anomalous contributions and CP-violating effects via a new asymmetry, *Phys. Rev. D* 107 (11) (2023) 115031. arXiv:[2301.13127](https://arxiv.org/abs/2301.13127), doi:[10.1103/PhysRevD.107.115031](https://doi.org/10.1103/PhysRevD.107.115031).
- [17] Q.-H. Cao, B. Yan, C. P. Yuan, Y. Zhang, Probing $Zt\bar{t}$ couplings using Z boson polarization in ZZ production at hadron colliders, *Phys. Rev. D* 102 (5) (2020) 055010. arXiv:[2004.02031](https://arxiv.org/abs/2004.02031), doi:[10.1103/PhysRevD.102.055010](https://doi.org/10.1103/PhysRevD.102.055010).
- [18] C. Severi, C. D. E. Boschi, F. Maltoni, M. Sioli, Quantum tops at the LHC: from entanglement to Bell inequalities, *Eur. Phys. J. C* 82 (4) (2022) 285. arXiv:[2110.10112](https://arxiv.org/abs/2110.10112), doi:[10.1140/epjc/s10052-022-10245-9](https://doi.org/10.1140/epjc/s10052-022-10245-9).
- [19] J. A. Aguilar-Saavedra, A. Bernal, J. A. Casas, J. M. Moreno, Testing entanglement and Bell inequalities in $H\rightarrow ZZ$, *Phys. Rev. D* 107 (1) (2023) 016012. arXiv:[2209.13441](https://arxiv.org/abs/2209.13441), doi:[10.1103/PhysRevD.107.016012](https://doi.org/10.1103/PhysRevD.107.016012).
- [20] J. A. Aguilar-Saavedra, Laboratory-frame tests of quantum entanglement in $H\rightarrow WW$, *Phys. Rev. D* 107 (7) (2023) 076016. arXiv:[2209.14033](https://arxiv.org/abs/2209.14033), doi:[10.1103/PhysRevD.107.076016](https://doi.org/10.1103/PhysRevD.107.076016).
- [21] M. Fabbrichesi, R. Floreanini, E. Gabrielli, L. Marzola, Bell inequalities and quantum entanglement in weak gauge boson production at the LHC and future colliders, *Eur. Phys. J. C* 83 (9) (2023) 823. arXiv:[2302.00683](https://arxiv.org/abs/2302.00683), doi:[10.1140/epjc/s10052-023-11935-8](https://doi.org/10.1140/epjc/s10052-023-11935-8).
- [22] R. Ashby-Pickering, A. J. Barr, A. Wierzychucka, Quantum state tomography, entanglement detection and Bell violation prospects in weak decays of massive particles, *JHEP* 05 (2023) 020. arXiv:[2209.13990](https://arxiv.org/abs/2209.13990), doi:[10.1007/JHEP05\(2023\)020](https://doi.org/10.1007/JHEP05(2023)020).
- [23] B. Henning, D. Lombardo, M. Riembau, F. Riva, Measuring Higgs Couplings without Higgs Bosons, *Phys. Rev. Lett.* 123 (18) (2019) 181801. arXiv:[1812.09299](https://arxiv.org/abs/1812.09299), doi:[10.1103/PhysRevLett.123.181801](https://doi.org/10.1103/PhysRevLett.123.181801).
- [24] D. R. Green, P. Meade, M.-A. Pleier, Multiboson interactions at the LHC, *Rev. Mod. Phys.* 89 (3) (2017) 035008. arXiv:[1610.07572](https://arxiv.org/abs/1610.07572), doi:[10.1103/RevModPhys.89.035008](https://doi.org/10.1103/RevModPhys.89.035008).
- [25] C. F. Anders, et al., Vector boson scattering: Recent experimental and theory developments, *Rev. Phys.* 3 (2018) 44–63. arXiv:[1801.04203](https://arxiv.org/abs/1801.04203), doi:[10.1016/j.revip.2018.11.001](https://doi.org/10.1016/j.revip.2018.11.001).
- [26] R. K. Ellis, et al., *Physics Briefing Book: Input for the European Strategy for Particle Physics Update 2020* (10 2019). arXiv:[1910.11775](https://arxiv.org/abs/1910.11775).

- [27] 2020 Update of the European Strategy for Particle Physics, CERN Council, Geneva, 2020. [doi: 10.17181/ESU2020](https://doi.org/10.17181/ESU2020).
- [28] R. Covarelli, M. Pellen, M. Zaro, Vector-Boson scattering at the LHC: Unraveling the electroweak sector, *Int. J. Mod. Phys. A* 36 (16) (2021) 2130009. [arXiv:2102.10991](https://arxiv.org/abs/2102.10991), [doi:10.1142/S0217751X2130009X](https://doi.org/10.1142/S0217751X2130009X).
- [29] D. Buarque Franzosi, et al., Vector boson scattering processes: Status and prospects, *Rev. Phys.* 8 (2022) 100071. [arXiv:2106.01393](https://arxiv.org/abs/2106.01393), [doi:10.1016/j.revip.2022.100071](https://doi.org/10.1016/j.revip.2022.100071).
- [30] A. Aeppli, F. Cuyppers, G. J. van Oldenborgh, O(Gamma) corrections to W pair production in e+ e- and gamma gamma collisions, *Phys. Lett. B* 314 (1993) 413–420. [arXiv:hep-ph/9303236](https://arxiv.org/abs/hep-ph/9303236), [doi:10.1016/0370-2693\(93\)91259-P](https://doi.org/10.1016/0370-2693(93)91259-P).
- [31] A. Aeppli, G. J. van Oldenborgh, D. Wyler, Unstable particles in one loop calculations, *Nucl. Phys. B* 428 (1994) 126–146. [arXiv:hep-ph/9312212](https://arxiv.org/abs/hep-ph/9312212), [doi:10.1016/0550-3213\(94\)90195-3](https://doi.org/10.1016/0550-3213(94)90195-3).
- [32] A. Denner, S. Dittmaier, M. Roth, D. Wackerth, Electroweak radiative corrections to e+ e- -> W W -> 4 fermions in double pole approximation: The RACOONWW approach, *Nucl. Phys. B* 587 (2000) 67–117. [arXiv:hep-ph/0006307](https://arxiv.org/abs/hep-ph/0006307), [doi:10.1016/S0550-3213\(00\)00511-3](https://doi.org/10.1016/S0550-3213(00)00511-3).
- [33] M. Billoni, S. Dittmaier, B. Jäger, C. Speckner, Next-to-leading order electroweak corrections to pp -> W+W- -> 4 leptons at the LHC in double-pole approximation, *JHEP* 12 (2013) 043. [arXiv:1310.1564](https://arxiv.org/abs/1310.1564), [doi:10.1007/JHEP12\(2013\)043](https://doi.org/10.1007/JHEP12(2013)043).
- [34] A. Denner, G. Pelliccioli, NLO EW and QCD corrections to polarized ZZ production in the four-charged-lepton channel at the LHC, *JHEP* 10 (2021) 097. [arXiv:2107.06579](https://arxiv.org/abs/2107.06579), [doi:10.1007/JHEP10\(2021\)097](https://doi.org/10.1007/JHEP10(2021)097).
- [35] D. N. Le, J. Baglio, Doubly-polarized WZ hadronic cross sections at NLO QCD + EW accuracy, *Eur. Phys. J. C* 82 (10) (2022) 917. [arXiv:2203.01470](https://arxiv.org/abs/2203.01470), [doi:10.1140/epjc/s10052-022-10887-9](https://doi.org/10.1140/epjc/s10052-022-10887-9).
- [36] A. Denner, C. Haitz, G. Pelliccioli, NLO EW corrections to polarised W+W- production and decay at the LHC, *Phys. Lett. B* 850 (2024) 138539. [arXiv:2311.16031](https://arxiv.org/abs/2311.16031), [doi:10.1016/j.physletb.2024.138539](https://doi.org/10.1016/j.physletb.2024.138539).
- [37] T. N. Dao, D. N. Le, NLO electroweak corrections to doubly-polarized W+W- production at the LHC, *Eur. Phys. J. C* 84 (3) (2024) 244. [arXiv:2311.17027](https://arxiv.org/abs/2311.17027), [doi:10.1140/epjc/s10052-024-12579-y](https://doi.org/10.1140/epjc/s10052-024-12579-y).
- [38] G. Pelliccioli, G. Zanderighi, Polarised-boson pairs at the LHC with NLOPS accuracy, *Eur. Phys. J. C* 84 (1) (2024) 16. [arXiv:2311.05220](https://arxiv.org/abs/2311.05220), [doi:10.1140/epjc/s10052-023-12347-4](https://doi.org/10.1140/epjc/s10052-023-12347-4).
- [39] M. Pellen, R. Poncelet, A. Popescu, Polarised W+j production at the LHC: a study at NNLO QCD accuracy, *JHEP* 02 (2022) 160. [arXiv:2109.14336](https://arxiv.org/abs/2109.14336), [doi:10.1007/JHEP02\(2022\)160](https://doi.org/10.1007/JHEP02(2022)160).
- [40] R. Poncelet, A. Popescu, NNLO QCD study of polarised W+W- production at the LHC, *JHEP* 07 (2021) 023. [arXiv:2102.13583](https://arxiv.org/abs/2102.13583), [doi:10.1007/JHEP07\(2021\)023](https://doi.org/10.1007/JHEP07(2021)023).
- [41] A. Ballestrero, A. Belhouari, G. Bevilacqua, V. Kashkan, E. Maina, PHANTOM: A Monte Carlo event generator for six parton final states at high energy colliders, *Comput. Phys. Commun.* 180 (2009) 401–417. [arXiv:0801.3359](https://arxiv.org/abs/0801.3359), [doi:10.1016/j.cpc.2008.10.005](https://doi.org/10.1016/j.cpc.2008.10.005).
- [42] A. Ballestrero, D. Buarque Franzosi, L. Oggero, E. Maina, Vector Boson scattering at the LHC: counting experiments for unitarized models in a full six fermion approach, *JHEP* 03 (2012) 031. [arXiv:1112.1171](https://arxiv.org/abs/1112.1171), [doi:10.1007/JHEP03\(2012\)031](https://doi.org/10.1007/JHEP03(2012)031).
- [43] A. Ballestrero, E. Maina, G. Pelliccioli, W boson polarization in vector boson scattering at the LHC, *JHEP* 03 (2018) 170. [arXiv:1710.09339](https://arxiv.org/abs/1710.09339), [doi:10.1007/JHEP03\(2018\)170](https://doi.org/10.1007/JHEP03(2018)170).
- [44] A. Ballestrero, E. Maina, G. Pelliccioli, Polarized vector boson scattering in the fully leptonic WZ and ZZ channels at the LHC, *JHEP* 09 (2019) 087. [arXiv:1907.04722](https://arxiv.org/abs/1907.04722), [doi:10.1007/JHEP09\(2019\)087](https://doi.org/10.1007/JHEP09(2019)087).
- [45] M. Hoppe, M. Schönherr, F. Siegert, Polarised cross sections for vector boson production with Sherpa, *JHEP* 04 (2024) 001. [arXiv:2310.14803](https://arxiv.org/abs/2310.14803), [doi:10.1007/JHEP04\(2024\)001](https://doi.org/10.1007/JHEP04(2024)001).
- [46] D. Buarque Franzosi, O. Mattelaer, R. Ruiz, S. Shil, Automated predictions from polarized matrix elements, *JHEP* 04 (2020) 082. [arXiv:1912.01725](https://arxiv.org/abs/1912.01725), [doi:10.1007/JHEP04\(2020\)082](https://doi.org/10.1007/JHEP04(2020)082).
- [47] F. Halzen, A. D. Martin, QUARKS AND LEPTONS: AN INTRODUCTORY COURSE IN MODERN PARTICLE PHYSICS, 1984.
- [48] S. Weinberg, The Quantum theory of fields. Vol. 1: Foundations, Cambridge University Press, 2005. [doi:10.1017/CB09781139644167](https://doi.org/10.1017/CB09781139644167).
- [49] R. Ruiz, A. Costantini, F. Maltoni, O. Mattelaer, The Effective Vector Boson Approximation in high-energy muon collisions, *JHEP* 06 (2022) 114. [arXiv:2111.02442](https://arxiv.org/abs/2111.02442), [doi:10.1007/JHEP06\(2022\)114](https://doi.org/10.1007/JHEP06(2022)114).

- [50] S. Dawson, The Effective W Approximation, Nucl. Phys. B 249 (1985) 42–60. doi:10.1016/0550-3213(85)90038-0.
- [51] G. L. Kane, W. W. Repko, W. B. Rolnick, The Effective W[±], Z0 Approximation for High-Energy Collisions, Phys. Lett. B 148 (1984) 367–372. doi:10.1016/0370-2693(84)90105-9.
- [52] Z. Kunszt, D. E. Soper, On the Validity of the Effective W Approximation, Nucl. Phys. B 296 (1988) 253–289. doi:10.1016/0550-3213(88)90673-6.
- [53] N. D. Christensen, C. Duhr, FeynRules - Feynman rules made easy, Comput. Phys. Commun. 180 (2009) 1614–1641. arXiv:0806.4194, doi:10.1016/j.cpc.2009.02.018.
- [54] N. D. Christensen, P. de Aquino, C. Degrande, C. Duhr, B. Fuks, M. Herquet, F. Maltoni, S. Schumann, A Comprehensive approach to new physics simulations, Eur. Phys. J. C 71 (2011) 1541. arXiv:0906.2474, doi:10.1140/epjc/s10052-011-1541-5.
- [55] C. Degrande, C. Duhr, B. Fuks, D. Grellscheid, O. Mattelaer, T. Reiter, UFO - The Universal FeynRules Output, Comput. Phys. Commun. 183 (2012) 1201–1214. arXiv:1108.2040, doi:10.1016/j.cpc.2012.01.022.
- [56] A. Alloul, N. D. Christensen, C. Degrande, C. Duhr, B. Fuks, FeynRules 2.0 - A complete toolbox for tree-level phenomenology, Comput. Phys. Commun. 185 (2014) 2250–2300. arXiv:1310.1921, doi:10.1016/j.cpc.2014.04.012.
- [57] C. Degrande, Automatic evaluation of UV and R2 terms for beyond the Standard Model Lagrangians: a proof-of-principle, Comput. Phys. Commun. 197 (2015) 239–262. arXiv:1406.3030, doi:10.1016/j.cpc.2015.08.015.
- [58] H. Murayama, I. Watanabe, K. Hagiwara, HELAS: HELicity amplitude subroutines for Feynman diagram evaluations (1 1992).
- [59] T. Stelzer, W. F. Long, Automatic generation of tree level helicity amplitudes, Comput. Phys. Commun. 81 (1994) 357–371. arXiv:hep-ph/9401258, doi:10.1016/0010-4655(94)90084-1.
- [60] T. Hahn, Generating Feynman diagrams and amplitudes with FeynArts 3, Comput. Phys. Commun. 140 (2001) 418–431. arXiv:hep-ph/0012260, doi:10.1016/S0010-4655(01)00290-9.
- [61] J. Alwall, R. Frederix, S. Frixione, V. Hirschi, F. Maltoni, O. Mattelaer, H. S. Shao, T. Stelzer, P. Torrielli, M. Zaro, The automated computation of tree-level and next-to-leading order differential cross sections, and their matching to parton shower simulations, JHEP 07 (2014) 079. arXiv:1405.0301, doi:10.1007/JHEP07(2014)079.
- [62] V. Hirschi, O. Mattelaer, Automated event generation for loop-induced processes, JHEP 10 (2015) 146. arXiv:1507.00020, doi:10.1007/JHEP10(2015)146.
- [63] A. Manohar, P. Nason, G. P. Salam, G. Zanderighi, How bright is the proton? A precise determination of the photon parton distribution function, Phys. Rev. Lett. 117 (24) (2016) 242002. arXiv:1607.04266, doi:10.1103/PhysRevLett.117.242002.
- [64] A. V. Manohar, P. Nason, G. P. Salam, G. Zanderighi, The Photon Content of the Proton, JHEP 12 (2017) 046. arXiv:1708.01256, doi:10.1007/JHEP12(2017)046.
- [65] V. Bertone, S. Carrazza, N. P. Hartland, J. Rojo, Illuminating the photon content of the proton within a global PDF analysis, SciPost Phys. 5 (1) (2018) 008. arXiv:1712.07053, doi:10.21468/SciPostPhys.5.1.008.
- [66] A. Buckley, J. Ferrando, S. Lloyd, K. Nordström, B. Page, M. Rüfenacht, M. Schönherr, G. Watt, LHAPDF6: parton density access in the LHC precision era, Eur. Phys. J. C 75 (2015) 132. arXiv:1412.7420, doi:10.1140/epjc/s10052-015-3318-8.
- [67] S. Alioli, S. Ferrario Ravasio, J. M. Lindert, R. Rötsch, Four-lepton production in gluon fusion at NLO matched to parton showers, Eur. Phys. J. C 81 (8) (2021) 687. arXiv:2102.07783, doi:10.1140/epjc/s10052-021-09470-5.
- [68] F. Caola, M. Dowling, K. Melnikov, R. Rötsch, L. Tancredi, QCD corrections to vector boson pair production in gluon fusion including interference effects with off-shell Higgs at the LHC, JHEP 07 (2016) 087. arXiv:1605.04610, doi:10.1007/JHEP07(2016)087.
- [69] G. Aad, et al., Evidence of off-shell Higgs boson production from ZZ leptonic decay channels and constraints on its total width with the ATLAS detector, Phys. Lett. B 846 (2023) 138223. arXiv:2304.01532, doi:10.1016/j.physletb.2023.138223.
- [70] M. Aaboud, et al., Constraints on off-shell Higgs boson production and the Higgs boson total width in $ZZ \rightarrow 4\ell$ and $ZZ \rightarrow 2\ell 2\nu$ final states with the ATLAS detector, Phys. Lett. B 786 (2018) 223–244. arXiv:1808.01191, doi:10.1016/j.physletb.2018.09.048.
- [71] A. Tumasyan, et al., Measurement of the Higgs boson width and evidence of its off-shell contributions to ZZ production, Nature Phys. 18 (11) (2022) 1329–1334. arXiv:2202.06923, doi:10.1038/s41567-022-01682-0.

- [72] G. Aad, et al., Evidence of pair production of longitudinally polarised vector bosons and study of CP properties in $ZZ \rightarrow 4\ell$ events with the ATLAS detector at $\sqrt{s} = 13$ TeV, *JHEP* 12 (2023) 107. [arXiv:2310.04350](#), [doi:10.1007/JHEP12\(2023\)107](#).
- [73] E. Bothmann, et al., Event Generation with Sherpa 2.2, *SciPost Phys.* 7 (3) (2019) 034. [arXiv:1905.09127](#), [doi:10.21468/SciPostPhys.7.3.034](#).
- [74] G. Aad, et al., Measurements of the Higgs boson inclusive and differential fiducial cross sections in the 4ℓ decay channel at $\sqrt{s} = 13$ TeV, *Eur. Phys. J. C* 80 (10) (2020) 942. [arXiv:2004.03969](#), [doi:10.1140/epjc/s10052-020-8223-0](#).
- [75] A. M. Sirunyan, et al., Measurements of production cross sections of the Higgs boson in the four-lepton final state in proton–proton collisions at $\sqrt{s} = 13$ TeV, *Eur. Phys. J. C* 81 (6) (2021) 488. [arXiv:2103.04956](#), [doi:10.1140/epjc/s10052-021-09200-x](#).
- [76] M. Cacciari, G. P. Salam, G. Soyez, The anti- k_t jet clustering algorithm, *JHEP* 04 (2008) 063. [arXiv:0802.1189](#), [doi:10.1088/1126-6708/2008/04/063](#).
- [77] G. Cowan, K. Cranmer, E. Gross, O. Vitells, Asymptotic formulae for likelihood-based tests of new physics, *Eur. Phys. J. C* 71 (2011) 1554, [Erratum: *Eur.Phys.J.C* 73, 2501 (2013)]. [arXiv:1007.1727](#), [doi:10.1140/epjc/s10052-011-1554-0](#).
- [78] Vector Boson Scattering prospective studies in the ZZ fully leptonic decay channel for the High-Luminosity and High-Energy LHC upgrades (2018).
- [79] G. Aad, et al., Observation of spin correlation in $t\bar{t}$ events from pp collisions at $\sqrt{s} = 7$ TeV using the ATLAS detector, *Phys. Rev. Lett.* 108 (2012) 212001. [arXiv:1203.4081](#), [doi:10.1103/PhysRevLett.108.212001](#).
- [80] A. J. Barr, P. Caban, J. Rembieliński, Bell-type inequalities for systems of relativistic vector bosons, *Quantum* 7 (2023) 1070. [arXiv:2204.11063](#), [doi:10.22331/q-2023-07-27-1070](#).
- [81] R. A. Morales, Exploring Bell inequalities and quantum entanglement in vector boson scattering, *Eur. Phys. J. Plus* 138 (12) (2023) 1157. [arXiv:2306.17247](#), [doi:10.1140/epjp/s13360-023-04784-7](#).
- [82] R. Aoude, E. Madge, F. Maltoni, L. Mantani, Probing new physics through entanglement in di-boson production, *JHEP* 12 (2023) 017. [arXiv:2307.09675](#), [doi:10.1007/JHEP12\(2023\)017](#).
- [83] J. A. Aguilar-Saavedra, Crafting polarizations for top, W, and Z, *Phys. Rev. D* 106 (11) (2022) 115021. [arXiv:2208.00424](#), [doi:10.1103/PhysRevD.106.115021](#).
- [84] G. Aad, et al., Observation of quantum entanglement in top-quark pairs using the ATLAS detector (11 2023). [arXiv:2311.07288](#).
- [85] M. L. Mangano, M. Moretti, F. Piccinini, R. Pittau, A. D. Polosa, ALPGEN, a generator for hard multiparton processes in hadronic collisions, *JHEP* 07 (2003) 001. [arXiv:hep-ph/0206293](#), [doi:10.1088/1126-6708/2003/07/001](#).
- [86] M. L. Mangano, M. Moretti, F. Piccinini, M. Treccani, Matching matrix elements and shower evolution for top-quark production in hadronic collisions, *JHEP* 01 (2007) 013. [arXiv:hep-ph/0611129](#), [doi:10.1088/1126-6708/2007/01/013](#).
- [87] T. Sjöstrand, S. Ask, J. R. Christiansen, R. Corke, N. Desai, P. Ilten, S. Mrenna, S. Prestel, C. O. Rasmussen, P. Z. Skands, An introduction to PYTHIA 8.2, *Comput. Phys. Commun.* 191 (2015) 159–177. [arXiv:1410.3012](#), [doi:10.1016/j.cpc.2015.01.024](#).
- [88] R. D. Ball, V. Bertone, S. Carrazza, L. Del Debbio, S. Forte, A. Guffanti, N. P. Hartland, J. Rojo, Parton distributions with QED corrections, *Nucl. Phys. B* 877 (2013) 290–320. [arXiv:1308.0598](#), [doi:10.1016/j.nuclphysb.2013.10.010](#).
- [89] M. Cacciari, G. P. Salam, Dispelling the N^3 myth for the k_t jet-finder, *Phys. Lett. B* 641 (2006) 57–61. [arXiv:hep-ph/0512210](#), [doi:10.1016/j.physletb.2006.08.037](#).
- [90] M. Cacciari, G. P. Salam, G. Soyez, Fast-Jet User Manual, *Eur. Phys. J. C* 72 (2012) 1896. [arXiv:1111.6097](#), [doi:10.1140/epjc/s10052-012-1896-2](#).